*J. Fluid Mech.* (2001), *vol.* 438, *pp.* 339–362. Printed in the United Kingdom



# Unsteady Stokes flow near an oscillating, heated contact line

By B. S. TILLEY[1], S. H. DAVIS[2] AND S. G. BANKOFF[3]

[1]Department of Mathematical Sciences, Center for Applied Mathematics and Statistics, New Jersey Institute of Technology, Newark, NJ 07102, USA

[2]Department of Engineering Sciences and Applied Mathematics, Northwestern University, Evanston, IL 60208, USA

[3]Department of Chemical Engineering, Northwestern University, Evanston, IL 60208, USA

(Received 24 October 1996 and in revised form 31 October 2000)

A contact line on a heated oscillating plate is investigated. The interface is a non-deformable plane and the contact angle is $\pi/2$. The amplitude of the oscillation and the temperature deviation of the plate from the ambient temperature of the fluid are assumed to be much smaller than the viscous velocity scale. This flow is then governed by the unsteady Stokes equations coupled to the heat equation in a frame of reference moving with the contact line. Evaporation is assumed to be neglible, but the effects of heat transfer across the interface and unsteadiness are assumed to be significant. For a stationary heated plate, there are two distinct regions of flow that is induced by Marangoni stresses. An outer stagnation-point-type flow is seen, which separates from the plate for non-zero Biot numbers. For an oscillatory, isothermal plate, vortices are generated at the plate during plate reversal and are propagated along the interface. Dissipation of these vortices occurs on the Stokes layer scale. The order-Péclet-number correction in the thermal field is also found, and the presence of the flow field leads to a heated region in the steady case along the separating streamline. For the unsteady case, a localized cooled region propagates into the bulk with a trajectory determined by the relative scale of the thermal diffusive scale and the rate of heat transfer across the interface.

## 1. Introduction

There are three length scales that are involved when one considers the flow near a contact line. One scale is that of the container size, or of the fluid motion within the bulk. A second is near the meniscus, where capillary forces balance viscous effects. The third is where viscous effects dominate, and the fluid motion is governed by the flow of a fluid in a wedge (Anderson & Davis 1993). In order to understand the motion of the fluid on each scale, each flow problem must be solved, and the resulting solutions need to be matched asymptotically.

When the interface between two fluids makes contact with a solid boundary, the application of the no-slip boundary condition results in a singularity in the stress at the contact line. This singularity is integrable if the contact line is fixed and the contact angle is allowed to vary. When the interface moves along the solid boundary, the no-slip boundary condition results in a non-integrable stress singularity (see Dussan V. & Davis 1974). One means of resolving this singularity is to allow the contact line

to slip locally. Although the local physics in the region is subject to debate, Dussan V. (1976) and Cox (1986) showed that the *outer flow* in a wedge of fluid near a steadily moving plate is independent of the details of the prescribed velocity conditions along the solid plate, each of which allows for slip at the contact line.

Anderson & Davis (1994) considered a contact-line region in a temperature gradient. They examined the degree of the fluid stress singularity as a function of the thermal stress singularity, where the temperature is governed by the heat equation, and the boundary conditions at the plate and interface are either no-flux or fixed constant temperature. They found that the flow forced by thermocapillarity is regular near the contact line.

In the present work, we examine a moving contact line on a heated plate, with a contact angle at the fixed value $\pi/2$. We prescribe a spatially varying plate temperature which fixes the temperature of the contact line at its ambient value, and approaches the far-field plate temperature away from the contact line. This plate temperature distribution eliminates the thermal-stress singularity at the contact line, and with Newton's law of cooling applied along the interface, the solution of this thermal problem results in an interfacial temperature profile with a heated region local to the contact line, and approaches the ambient temperature far from the contact line. The temperature gradient induces a Marangoni-driven flow that, as we shall see, has two distinct regions: an outer forward stagnation-point flow along the interface to the contact line, which separates from the plate a few thermal lengths away from the contact line; and past this flow separation point, there is a reverse flow along the plate toward the separating streamline.

Further, in the same spirit as Dussan V. (1976) we consider here the contact-line region in cases where the outer flow has significant unsteadiness. In the past the local wedge flow has been taken to be quasi-steady; see for example Dussan V. & Davis (1974), Hocking (1987*b*), Miles (1990 *a*, *b*), Miles (1991), and Sheng & Zhou (1992). Although the vertical contact line is a special case, it does allow standard techniques to be applied for its solution. Hence, the focus of this paper is to understand when the unsteady nature of the local flow is pertinent to the outer flow. We study the purely oscillatory moving vertical contact line, and find that there is a region of flow reversal that is generated along the plate. On a viscous time scale, the region of flow reversal leads to the propagation of a vortex within the bulk of the fluid: a capillary ripple. This ripple decays within an unsteady Stokes boundary layer. We shall see that no matter how small the frequency of oscillation of the plate is, this phenomenon persists. Such damping behaviour for surface waves has also been investigated with brimful cylinders, both experimentally and theoretically (see Benjamin & Scott 1979; Henderson & Miles 1994; Martel, Nicolás & Vega 1998; Miles & Henderson 1998; Perlin & Schultz 2000).

From the solution of each of these flow fields in the limit of zero Reynolds number, we find the correction to the thermal field due to the Marangoni-induced flow and the oscillating-plate-induced flow. The steady flow produces a heated region along a separating streamline, with maximum cooling of the plate due to advective effects occurring when heat conducts poorly from the liquid to the environment. The unsteady plate propagates a cooled localized region into the bulk, depending on the relative measure of heat loss through the interface and advective heat transport.

We begin with the formulation of the problem in § 2. In § 3, we report on the flow and thermal fields to leading order in Reynolds number. In § 4 we investigate the thermal field induced by the leading-order steady-state and oscillatory flow components. We conclude in § 5.

## 2. Unsteady Stokes flow with periodic forcing on a heated plate

We are interested primarily in how both unsteadiness and thermocapillarity affect the liquid flow, dominated by viscous effects, local to a contact line between a viscous fluid and a passive gas. To best isolate these effects, it is useful to consider a physical situation where other effects, such as differences in advancing and receding contact angles or interfacial deformation, are ignored, and the time-harmonic solutions are found. In the formulation that follows, we start with the full equations of motion, and then successively introduce restrictions on the fluid problem so that the fluid flow to leading order in the zero-Reynolds-number limit is coupled to the thermal problem only through Marangoni stresses at the interface. Additional effects can be readily included in the following formulation for more general situations.

Consider the flow in a 90° wedge of incompressible, viscous liquid bounded by a solid heated surface and a passive gas as shown in figure 1. We assume that the no-slip boundary condition is relaxed on the plate near the contact line by posing a slip velocity analogous to that of Dussan V. (1976). In a frame of reference moving with the contact line, the flow within the wedge is governed by the continuity, energy and Navier–Stokes equations

$$\nabla \cdot \boldsymbol{u} = 0,$$

$$T_t - a'(t)T_x + \boldsymbol{u} \cdot \nabla T = \kappa \nabla^2 T,$$

$$\boldsymbol{u}_t - a'(t)\boldsymbol{u}_x + \boldsymbol{u} \cdot \nabla \boldsymbol{u} = -\frac{1}{\rho}\nabla p + \nu \nabla^2 \boldsymbol{u},$$

where $\boldsymbol{u}$ is the fluid velocity, $T$ is the fluid temperature, $p$ is the pressure, $a(t)$ is the contact-line location in the laboratory frame, $\kappa$ is the thermal diffusivity, $\rho$ is the density, and $\nu$ is the kinematic viscosity. At the interface, $x = h(y,t)$, we require continuity of mass and energy, and the jump in shear stress is balanced by thermocapillarity. We assume that the interface remains flat (i.e. consider partial local solutions), and that there is no evaporation of the liquid into the gas. Thus,

$$h_t + v h_y - u = 0, \tag{2.1}$$

$$k \nabla T \cdot \boldsymbol{n} + b(T - T_a) = 0, \tag{2.2}$$

$$2\mu \boldsymbol{t} \cdot \boldsymbol{T} \cdot \boldsymbol{n} = \nabla \sigma \cdot \boldsymbol{t}, \tag{2.3}$$

where $T_a$ is the ambient temperature, $b$ is the heat transfer coefficient, $\mu$ is the dynamic viscosity of the liquid, $\boldsymbol{T}$ is the rate-of-deformation tensor, $\boldsymbol{n}$, $\boldsymbol{t}$ are the normal and tangential vectors at the interface, respectively, and $\sigma = \sigma_0 - \gamma(T - T_a)$ is the temperature-dependent surface tension. The normal-stress boundary condition is ignored, since we are interested in partial local solutions (see Anderson & Davis 1993). We prescribe a tangential velocity profile on the solid boundary at $y = 0$

$$u(x,0,t) = U_w(x)\cos \omega t,$$
$$v(x,0,t) = 0,$$

where $(u,v)$ are the $(x,y)$ velocity components. The prescribed velocity profile $U_w(x)$ is assumed to be zero at $x = 0$ and approaches a general constant velocity $U$ as $x$ increases. The transition scale from perfect slip at the contact line to no-slip away from the contact line occurs on a prescribed length scale $L_s$.

The thermal problem also possesses a singularity near the contact line if the plate temperature is not the same as the ambient temperature of the gas. There are several methods of eliminating this singularity, two of which are allowing the plate to have

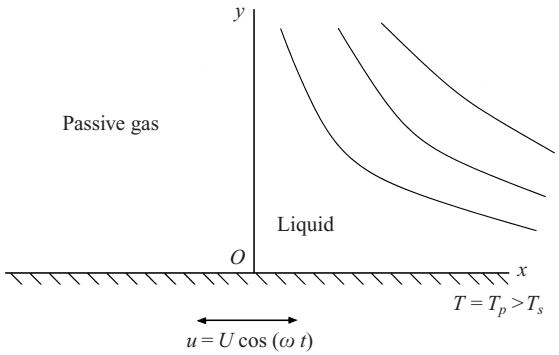


FIGURE 1. Problem configuration for Stokes flow near an oscillatory contact line on a heated plate.

some finite thickness, or prescribing a spatially dependent temperature profile along the plate; we choose the second alternative. The profile used in this work fixes the contact-line temperature to be the ambient temperature

$$T_w(x) = T_p + (T_a - T_p)\mathrm{e}^{-x/L_T}. \tag{2.4}$$

The length scale of the thermal boundary layer local to the contact line, $L_T$, is one characteristic scale of the flow generated by Marangoni effects.

We scale lengths on the thermal length scale $L_T$, and velocities on the amplitude $U$ of the forcing of the flow. We assume in the thermal problem that this scale depends linearly on the temperature deviation of the plate from the ambient temperature of the fluid. In the oscillatory problem, this scale is the amplitude of the plate oscillation. In both cases, we assume that this scale is much smaller than the viscous velocity scale $L_T/\nu$. We scale time on the period of the oscillation $1/\omega$, pressure on the Stokes scale $\mu U/L_T$, and temperature is redefined as $\Theta = (T - T_a)/\Delta T$, $\Delta T = T_p - T_a$, to arrive at the following scaled system

$$\nabla \cdot \boldsymbol{u} = 0,$$

$$S\boldsymbol{u}_t - Sa'(t)\boldsymbol{u}_x + Re\boldsymbol{u}\cdot\nabla\boldsymbol{u} = -\nabla p + \nabla^2\boldsymbol{u},$$

$$SP\Theta_t - SPa'(t)\Theta_x + Pe\boldsymbol{u}\cdot\nabla\Theta = \nabla^2\Theta,$$

where $S = L_T^2\omega/\nu$ is the Strouhal number, $Re = UL_T/\nu \ll 1$ is the Reynolds number, $P = \nu/\kappa$ is the Prandtl number, and $Pe = ReP = UL_T/\kappa$ is the Péclet number. The interfacial conditions (2.1)–(2.3) at $x = h(y,t)$ become

$$Sh_t + Re(vh_y - u) = 0, \tag{2.5}$$

$$\nabla\Theta\cdot\boldsymbol{n} + B\Theta = 0, \tag{2.6}$$

$$\boldsymbol{n}\cdot\boldsymbol{T}\cdot\boldsymbol{t} = -M\nabla\Theta\cdot\boldsymbol{t}, \tag{2.7}$$

where $B = L_T b/k$ is the Biot number, and $M = \gamma\Delta T/(\mu U)$ is the Marangoni number. This formulation corresponds to the zero evaporation and capillary limits of Burelbach, Bankoff & Davis (1988), with $B = 1/K$ being the inverse of the disequilibrium parameter.

Along the plate the prescribed velocity profile becomes

$$u(x,0,t) = u_w(x)\cos t,$$
$$v(x,0,t) = 0,$$

with the prescribed velocity $u_w(x) \to 1$ as $x \to \infty$. The temperature condition along the plate becomes $\Theta = \theta_w(x)$.

The problem for $S = Re = 0$ is the steady wedge flow studied by Dussan V. (1976) which represents the local flow near a steadily moving, isothermal contact line. We wish to study local effects near a contact line that is strongly unsteady, or that is weakly thermally driven ($M = O(1)$). We assume that the inertial effects are small, $Re \to 0$, and that time variations can be significant ($S, P = O(1)$), and we assume that curvature is zero along the interface $h_y = 0$. These conditions require that the interface remain fixed at $h(y,t) = 0$, hence $a'(t) = 0$ for the time scales that are of interest here, and that the normal velocity of the liquid vanishes at the interface.

We expand the streamfunction $\psi$, defined by $\boldsymbol{u} = \psi_y \boldsymbol{i} - \psi_x \boldsymbol{j}$, and the temperature $\Theta$ as a regular asymptotic expansion in Reynolds number

$$\psi(x,y,t) = \psi_0(x,y,t) + Re\psi_1(x,y,t) + Re^2\psi_2(x,y,t) + \cdots,$$
$$\Theta(x,y,t) = \Theta_0(x,y,t) + Re\Theta_1(x,y,t) + Re^2\Theta_2(x,y,t) + \cdots,$$

and the resulting leading-order flow problem in $Re$ becomes

$$S(\nabla^2\psi_0)_t = \nabla^4\psi_0, \quad SP\Theta_{0t} = \nabla^2\Theta_0, \tag{2.8}$$

with $\psi_0 = 0$, $\psi_{0y} = u_0(x)\cos t$, and $\Theta_0 = \Theta_0(x)$ along the plate $y = 0$. The interfacial conditions (2.5)–(2.7) are now evaluated at $x = 0$ and are

$$\psi_0 = 0, \tag{2.9}$$

$$\Theta_{0x} - B\Theta_0 = 0, \tag{2.10}$$

$$\psi_{0xx} = -2M\Theta_{0y}. \tag{2.11}$$

We note that there are two forcings on the flow field. One is the flow induced by the oscillating plate, while the second is driven by Marangoni stresses at the interface. Since the problem (2.8)–(2.11) is linear, we can investigate the resulting flow under each forcing individually, and use the principle of superposition to find the solution in the general case. In both cases, we are primarily concerned with the long-time solution of the flow and thermal fields after the initial transients have decayed to zero.

## 3. Leading-order solutions

### 3.1. *Thermocapillary flow with a stationary contact line*

Consider the flow that is generated by Marangoni stresses induced by thermal gradients. Since the thermal field is decoupled from the flow field, we can solve the thermal problem directly, and find the resulting flow field. The thermal problem is

$$SP\Theta_{0t} = \nabla^2\Theta_0,$$

with $\Theta = \theta_w(x)$ along $y = 0$; $\theta_w(x)$ is a prescribed temperature profile with $\theta_w(0) = 0$, so that there is no singularity in the thermal stress at the contact line. Anderson & Davis (1993) considered Marangoni-induced flows when the plate temperature was either uniform in $x$ or the heat flux through the plate was uniform in $x$. We shall see that the present approach leads to a non-uniform interfacial temperature profile as $y \to 0$. Note that since the boundary conditions are steady, and since we are only considering the long-time solution of the flow, only the steady-state solution is

needed. This problem can be solved using standard techniques, so we shall assume that we can find the thermal field $\Theta_0(x, y)$ which satisfies the above system.

Since the thermal field is steady, the Marangoni stress on the interface is steady, suggesting that the solution of the flow field due this effect is steady. The problem for the flow field is

$$\nabla^4\psi_0 = 0, \quad 0 < x, y < \infty, \tag{3.1}$$

$$\psi_0(x, 0) = 0, \tag{3.2}$$

$$\psi_{0y}(x, 0) = 0, \tag{3.3}$$

$$\psi_0(0, y) = 0, \tag{3.4}$$

$$\psi_{0xx}(0, y) = -2M\Theta_{0y}(0, y), \tag{3.5}$$

$$\psi_0, \psi_{0y} \to 0 \quad \text{as} \quad x, y \to \infty. \tag{3.6}$$

Applying the Fourier sine transform in $x$,

$$\bar{\psi} = \frac{2}{\pi}\int_0^\infty \psi_0(x, y)\sin\sigma x\mathrm{d}x,$$

$$\psi_0(x, y) = \int_0^\infty \bar{\psi}\sin\sigma x\mathrm{d}\sigma,$$

we arrive at the following ordinary differential equation:

$$\bar{\psi}_{yyyy} - 2\sigma^2\bar{\psi}_{yy} + \sigma^4\bar{\psi} = \frac{4}{\pi}\sigma M\Theta_y(0, y) \tag{3.7}$$

with $\bar{\psi} = 0, \bar{\psi}_y = 0$ at $y = 0$ and $\bar{\psi}, \bar{\psi}_y \to 0$ as $y \to \infty$. After applying the method of variation of parameters to the differential equation (3.7), the particular solution $\bar{\psi}_p$ is given by

$$\bar{\psi}_p(y, \sigma) = \frac{M}{\pi\sigma}\int_0^y \left[(y-\eta)\cosh[\sigma(y-\eta)] - \frac{1}{\sigma}\sinh[\sigma(y-\eta)]\right]\Theta_{0y}(0, \eta)\mathrm{d}\eta,$$

$$= \frac{M}{\pi}\int_0^y \Theta_0(0, \eta)(y-\eta)\sinh[\sigma(y-\eta)]\mathrm{d}\eta,$$

by using integration by parts and $\Theta_0(0, 0) = 0$. This particular solution grows exponentially as $y \to \infty$, so by adding the appropriate weights of the exponentially growing homogeneous solutions $\{\exp(\sigma y), y\exp(\sigma y)\}$, the full solution grows at most algebraically. With the boundary conditions at $x = 0$, the resulting solution can be written as

$$\bar{\psi} = \frac{M}{2\pi}\int_0^\infty \{(\eta - y)\mathrm{e}^{-\sigma|\eta-y|} + (y - \eta - 2\sigma\eta y)\mathrm{e}^{-\sigma(y+\eta)}\}\,\Theta_0(0, \eta)\mathrm{d}\eta. \tag{3.8}$$

The resulting flow, after inversion of the Fourier sine transform, is then found to be

$$\psi_0(x, y) = \frac{2M}{\pi}xy^2\int_0^\infty \eta\Theta_0(0, \eta)\frac{\eta^2 - (x^2+y^2)}{[x^2+(\eta-y)^2][x^2+(\eta+y)^2]^2}\mathrm{d}\eta. \tag{3.9}$$

As expected, when there is no dependence of surface tension on temperature ($M = 0$), there is no flow. From this solution, the force applied to the plate by the

liquid is then found to be

$$F(x) = \int_0^x -\psi_{yy}(\xi, 0)\mathrm{d}\xi$$
$$= -\frac{2M}{\pi}x^2 \int_0^\infty \Theta_0(0,\eta)\left\{\frac{\eta}{(\eta^2+x^2)^2}\right\}\mathrm{d}\eta. \tag{3.10}$$

Hence, the flow properties are determined by convolutions of the interfacial temperature and some descriptive kernel. In order to quantitatively study this flow solution, the solution to the thermal problem is needed. We let $\Theta_0(x,y) = \mathrm{e}^{-y}\theta_w(x) + \phi(x,y)$, where $\theta_w(x)$ is the general temperature profile along the plate, which results in a Poisson equation for $\phi$ with $\phi(x,0) = 0$ along the plate. The solution of the thermal problem, using the Fourier sine transform in $y$, gives

$$\Theta_0(x,y) = \frac{1}{\pi}\int_0^\infty [\theta_w''(\xi) + \theta_w(\xi)]\int_0^\infty \frac{\sin\sigma y}{\sigma^2+1}\left[\mathrm{e}^{-\sigma|x-\xi|} - \left(\frac{2B}{\sigma+B} - 1\right)\mathrm{e}^{-\sigma(x+\xi)}\right]\mathrm{d}\sigma\mathrm{d}\xi$$
$$+\mathrm{e}^{-y}\theta_w(x) + \frac{2[\theta_w'(0) - B\theta_w(0)]}{\pi}\int_0^\infty \frac{\sigma\sin(\sigma y)\mathrm{e}^{-\sigma x}}{(\sigma^2+1)(\sigma+B)}\mathrm{d}\sigma. \tag{3.11}$$

In the following, we consider the specific thermal profile $\theta_w(x) = 1 - \exp(-x)$. Since the flow problem is the primary interest, and this depends only on the interfacial temperature, setting $x = 0$ in (3.11) and performing the integrations leads to a closed-form solution for the interfacial temperature in this case:

$$\Theta_0(0,y) = \begin{cases} \dfrac{2}{\pi}\dfrac{f(y) - f(By)}{B-1}, & B \neq 1 \\ -\dfrac{2y}{\pi}\{-\sin y[\pi/2 - \mathrm{Si}(y)] + \cos y\ \mathrm{Ci}(y)\}, & B = 1, \end{cases}$$

$$f(z) = \mathrm{Ci}(z)\sin z + \cos z[\pi/2 - \mathrm{Si}(z)], \tag{3.12}$$

where $\mathrm{Ci}(x)$ and $\mathrm{Si}(x)$ are the cosine and sine integrals, respectively. The advantage of using the above forms for the interfacial temperature is that efficient numerical techniques are available (Press *et al.* 1992) that can determine these special functions to within roundoff error.

In figure 2, we show the interfacial temperature of this solution for the cases $B = 0, 0.1, 1, 10$. Notice that the temperature in the region closest to the plate is elevated, but then decays algebraically toward the ambient temperature as $y \to \infty$. The temperature decay to leading order is $\Theta_0(0,y) \sim 2/(B\pi y)$, for fixed $B \neq 0$, as $y \to \infty$, so that a smaller heat-transfer coefficient leads to larger interfacial temperatures, and hence a weaker transport of heat from the bulk to the environment. Note that the limit $B \to 0$ is a singular limit in the sense that the far-field interfacial temperature changes from $\Theta_0(0,y) \sim 0$ for $B \neq 0$ to $\Theta_0(0,y) \sim 1$ for $B = 0$ to leading order as $y \to \infty$. Near the contact line, the interfacial temperature behaves as $\Theta_0(0,y) \sim -2(y\ln y)/\pi + O(y)$ for all $B$, with the singularity in the second derivative due to the non-zero first derivative in the prescribed temperature profile on the plate $\theta_w(x)$. In dimensional form, this interfacial temperature is non-uniform as $L_T \to 0$.

For $B \neq 0$, the presence of the extremum in interfacial temperature leads to interfacial shear stresses from the extremum to the contact line and from the extremum to the far field. The difference in magnitude of these stresses is significant, with the

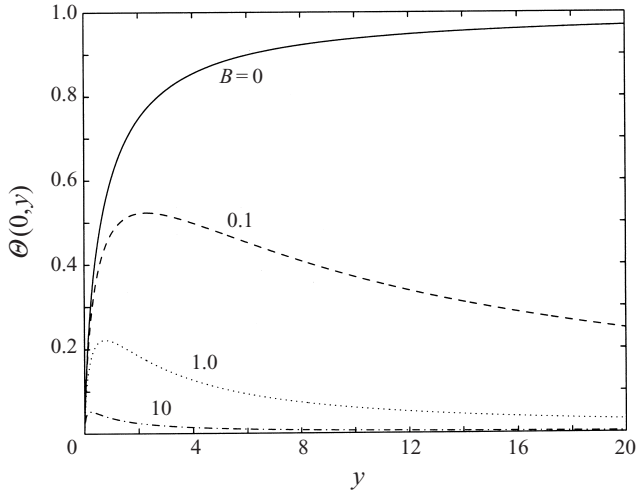


FIGURE 2. Interfacial temperature of the solution (3.11) for $B = 0, 0.1, 1$, and 10 with $\theta_w(x) = 1-\mathrm{e}^{-x}$. Note that the temperature decays to the ambient temperature algebraically as $y \to \infty$ for $B \neq 0$.

net result being flow along the interface into the contact line region. These inferences can be seen in figure 3 for the values $B = 0.1, 1, 10$. Figure 3($a$) shows the region local to the contact line, $0 < x, y < 5$, where the flow separation can be seen in detail. Figure 3($b$) shows the same flow over $0 < x, y < 50$, where the outer flow can be seen. These calculations were performed by splitting the infinite interval of integration into a finite part and a semi-infinite part. The semi-infinite part was transformed to a finite interval by the transformation $\bar{\eta} = 1/\eta$, and Romberg integration was used on each integral. Care was taken near the interface to avoid the singularity in the integral as $x \to 0$ by scaling $x, y, \eta$ on the non-zero value of $x$ and numerically integrating the result in the same manner.

Figure 4 shows the force along the plate as a function of distance from the contact line. Note that the force on the plate in the $B = 0$ case is bounded and reaches an asymptotic value of approximately $F_{min} \approx -0.32$. This shows that there is no appreciable stress on the plate beyond $x = 10$ for $B = 0$. For non-zero Biot numbers, the force along the plate decreases due to the reverse flow along the plate that is induced by the Marangoni stresses. The relative strength of this reverse flow is seen in figure 4 by the presence of a minimum force that decreases with increasing Biot number. In figure 5, we show the minimum value of the force along the plate as a function of Biot number, and the location along the plate at which this minimum is reached. Notice that the minimum value of the force decreases as $B \to \infty$, while the minimum location approaches zero in this limit.

Also of interest is the asymptotic behaviour of the liquid velocity at the interface as the contact line is approached. We find that the liquid velocity at the interface $v(0, y)$ is given by

$$v(0,y) = -\frac{2My^2}{\pi}\int_0^\infty \frac{\eta\Theta_0(0,\eta)}{(\eta-y)(\eta+y)^3}\mathrm{d}\eta \tag{3.13}$$

in terms of the principal-value integral. The leading-order velocity profile behaves like $v(0, y) \sim 4M(y \ln y)/\pi^2 + O(y)$ as $y \to 0$. The flow is independent of the Biot number since the interfacial temperature near $y = 0$ is to leading order independent of $B$.

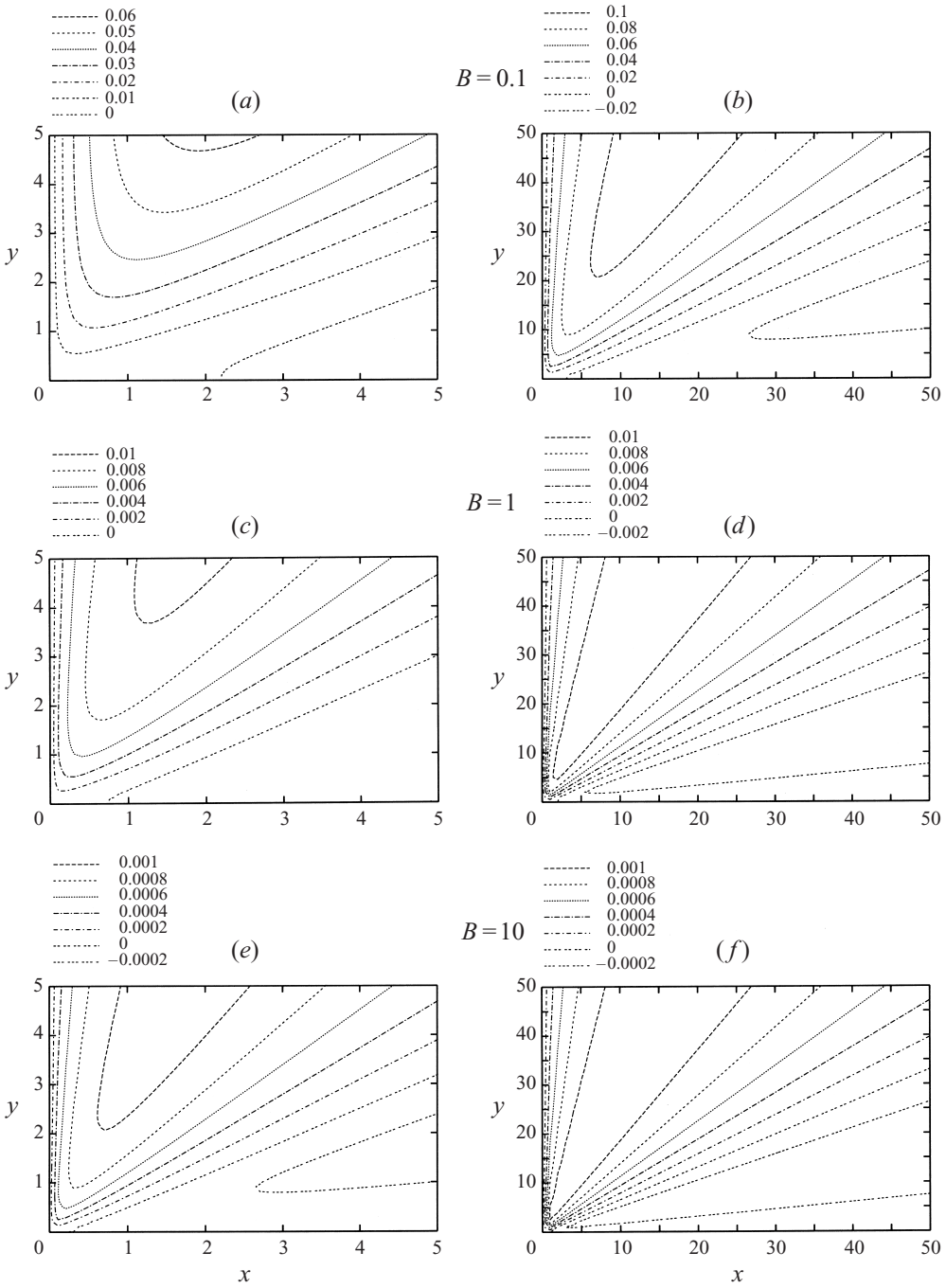


FIGURE 3. Contour plots of the streamfunction driven by thermocapillarity and heat transfer for $B = 0.1, 1$, and 10. (*a*) The region near the contact line showing the flow separation along the plate, (*b*) the outer flow, which moves in a counterclockwise sense above the flow separation line that intersects $x = 50$ in $30 < y < 35$, as is expected for the outer fluid driven by Marangoni stresses.

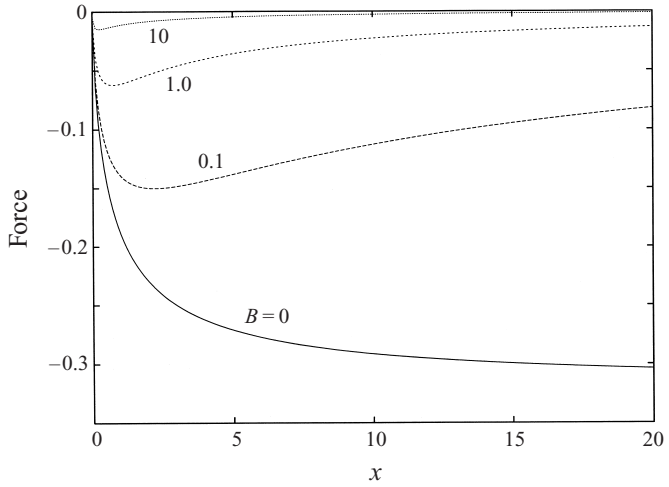


FIGURE 4. Force of the fluid acting on the plate $F(x)$ against distance from the contact line along the plate $x$ for Biot numbers $B = 0, 0.1, 1$, and 10. Note that the force approaches finite values as $x \to \infty$.

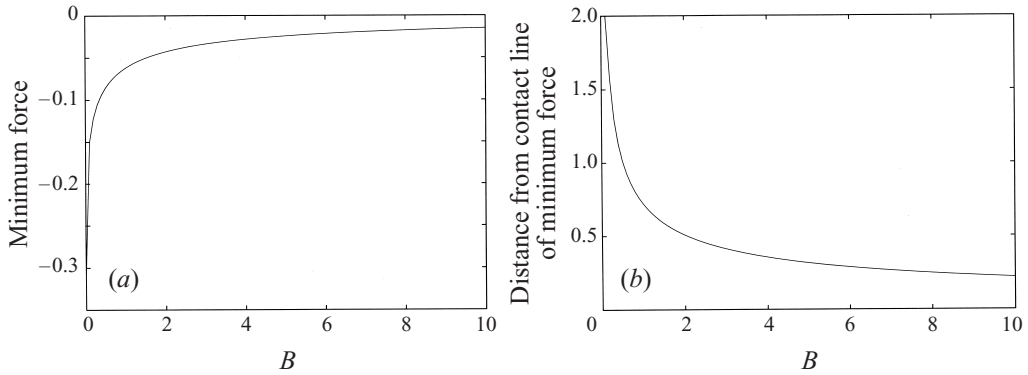


FIGURE 5. (*a*) Minimum force value as a function of the Biot number $B$. (*b*) The distance $x_{min}$ away from the contact line at which this force is obtained. The limit $B \to 0$ shows that the maximum value moves out towards infinity.

### 3.2. *Oscillating contact line in an isothermal liquid*

When $\Theta_0(x) = 0$ along the plate $y = 0$, the only solution to the thermal problem is the trivial solution $\Theta_0 = 0$. Hence, we only need to study the flow generated by the oscillating plate.

In the isothermal case, the interface is stress-free, $\psi_{0xx} = 0$ along $x = 0$. For general time-dependent forcing, however, the stress on the plate will depend on the history of the flow. If we integrate the unsteady Stokes equations once in time, we find that

$$\nabla^2\psi_0 = \nabla^2\psi_0\big|_{t=0} + \frac{1}{S}\int_0^t \nabla^4\psi_0 \mathrm{d}\bar{t}. \tag{3.14}$$

Along the plate $\psi_0 = 0$, implying that all purely radial derivatives vanish. If we note

that the shear stress along the plate is $\tau_0(x,t) = -\psi_{0yy}|_{y=0}$, and substitute for this expression, we find that

$$\tau_0(x,t) = \tau_0(x,0) + \frac{1}{S}\int_0^t \{\nabla^2\tau_0 + \tau_{0xx}\}\big|_{y=0}\,\mathrm{d}\bar{t}. \tag{3.15}$$

Thus, the stress along the plate is history dependent, and it is not clear if any boundary condition that is local in time (e.g. a Navier relation) is appropriate.

However, we expect that over long times the flow is in general dissipative, and the periodic long-time response of the flow should be independent of initial data if the plate is oscillating at a single frequency.

Thus, we solve the oscillatory problem with the slip condition

$$u_w(x) = 1 - \mathrm{e}^{-\beta x}, \tag{3.16}$$

where $\beta = L_s/L_T$ is the ratio of the slip length scale to the thermal length scale along the plate. This condition may not be appropriate for large frequencies of oscillation, since accelerations in time would then be significant, and a prescribed velocity condition, valid for steady flows, may not apply. In this subsection, we assume that $\beta = 1$, or equivalently $L_s = L_T$. Later, when we consider advective heat transport due to this flow, $\beta$ will not necessarily equal unity.

We are interested in the long-time solution of the flow, and we apply the Fourier sine transform in the $x$-coordinate, and solve the resulting ordinary differential equation in $y$. We define $\psi_0(x,y,t) = \hat{\psi}(x,y)\exp(\mathrm{i}t) + \text{c.c.}$, where c.c. denotes the complex conjugate, and apply the Fourier sine transform in $x$

$$\bar{\psi}(y,\sigma) = \frac{2}{\pi}\int_0^\infty \hat{\psi}(x,y)\sin\sigma x\,\mathrm{d}x,$$

$$\hat{\psi}(x,y) = \int_0^\infty \bar{\psi}(y,\sigma)\sin\sigma x\,\mathrm{d}\sigma.$$

The vorticity equation becomes

$$\bar{\psi}_{yyyy} - (2 + \mathrm{i}S\sigma^2)\bar{\psi}_{yy} + \sigma^2(\sigma^2 + \mathrm{i}S)\bar{\psi} = 0,$$
$$\bar{\psi}(0,\sigma) = 0,$$
$$\bar{\psi}_y(0,\sigma) = U_w(\sigma).$$

The solution to this system is

$$\bar{\psi} = \frac{U_w(\sigma)}{\sigma - \sqrt{\sigma^2 + \mathrm{i}S}}\{\exp(-y\sqrt{\sigma^2 + \mathrm{i}S}) - \mathrm{e}^{-\sigma y}\}, \tag{3.17}$$

which, after some manipulation, yields the following convolution integral solution for $\hat{\psi}$:

$$\hat{\psi}(x,y) = \frac{1}{2\pi\sqrt{1+\mathrm{i}S}}\int_0^\infty u_w(\xi)\left\{\ln\left[\frac{(1+\mathrm{i}S)y^2 + (x+\xi)^2}{(1+\mathrm{i}S)y^2 - (x-\xi)^2}\right] - \ln\left[\frac{y^2 + (x+\xi)^2}{y^2 - (x-\xi)^2}\right]\right\}\mathrm{d}\xi. \tag{3.18}$$

Although this solution may be somewhat simpler mathematically, it is numerically more efficient to perform the inverse Fourier sine transform numerically on the solution (3.17), since the integrand decays exponentially for $y \neq 0$.

Figure 6 shows the streamlines for the flow field for $0 < x, y < 10$ at various times from $t = \pi/16$ to $t = \pi$ with $S = 0.1$. Initially the flow resembles a single vortex. As the plate decelerates to a stop at $t = \pi/2$, the flow is still moving in a clockwise sense about the centre streamline. As the plate reverses, a second vortex appears local to the plate, with the flow moving in a counter-clockwise sense. The strength of this vortex pushes the dissipating positively sensed vortex away from the plate, until this new vortex dominates the flow at $t = \pi$.

Figure 7 displays the effect of the dissipating vortex more globally, with $S = 1$ on $0 < x, y < 10$ and at various times from $t = \pi/16$ to $t = 13\pi/16$. Since the period of oscillation is nearly the same as the vorticity-diffusion time scale, the vortex dissipates more quickly than in the $S = 0.1$ case. As the plate reverses direction, the second vortex develops and the zero streamline, separating the two vortices as in the $S = 0.1$ case, but at $t = 13\pi/16$, enclosing the positively sensed vortex. This vortex has more clearly propagated further in the vertical direction as is shown at time $t = 11\pi/16$. This is the effect of the Stokes layer: for small Strouhal numbers, the Stokes layer is relatively thick, and the scale of dissipation is of the order $S^{-1/2}$. As $S \to \infty$, viscosity dominates over unsteadiness, and the propagating vortex decays more quickly.

The force of the fluid on the plate at a particular location $x$ from the contact line is now a periodic function of time

$$F(x,t) = -\int_0^x \left[\hat{\psi}_{yy} e^{it} + \text{c.c.}\right]\Big|_{y=0} \mathrm{d}x. \tag{3.19}$$

Hence, the appropriate quantities to investigate are the amplitude of the force and the phase difference the force with respect to the plate oscillation. In figure 8, the amplitude of the force with respect to the distance $x$ from the contact line for Strouhal numbers $S = 0.1, 1, 10$ is shown. We see that the force appears to grow sub-algebraically, as in the thermal problem. The phase of the force with respect to the plate is shown in figure 9, where the phase lag is expected due to the slipping contact line. Figure 10 shows the amplitude of the force plotted against Strouhal number at the spatial location $x = 1000$. we see that the amplitude of the force fits, roughly, a square-root curve, which coincides with the dissipation-rate scale of $v^{1/2}$ found in the literature (see Mei & Liu 1973 or Hocking 1987*a* for example).

We have investigated the liquid velocity at the interface of $\hat{\psi}$ as $y \to 0$, and found that $\hat{v}(0,y) \sim -u_w(y)/(2\sqrt{1+\mathrm{i}S}) + O(yu'_w(y))$. This result is found by taking the $x$-derivative of (3.18) and finding the singular contribution of the integral as $x \to 0$.

## 4. Heat transport

The flow generated by Marangoni forces on the interface and the oscillatory motion of the plate results in a change of heat flow of order $Re$. To determine this correction quantitatively, the thermal problem at $O(Pe)$, with $Re \to 0$, needs to be solved. From the asymptotic expansion above, this problem is stated as

$$\begin{aligned} SP\Theta_{1t} - \nabla^2\Theta_1 &= -P\boldsymbol{u}_0 \cdot \nabla\Theta_0 \\ &= -PJ(\psi_0, \Theta_0), \end{aligned} \tag{4.1}$$

with $\Theta_{1x} - B\Theta_1 = 0$ at $x = 0$, and $\Theta_1 = 0$ along $y = 0$.

The solution to this problem is standard: we use the Fourier sine transform in $y$

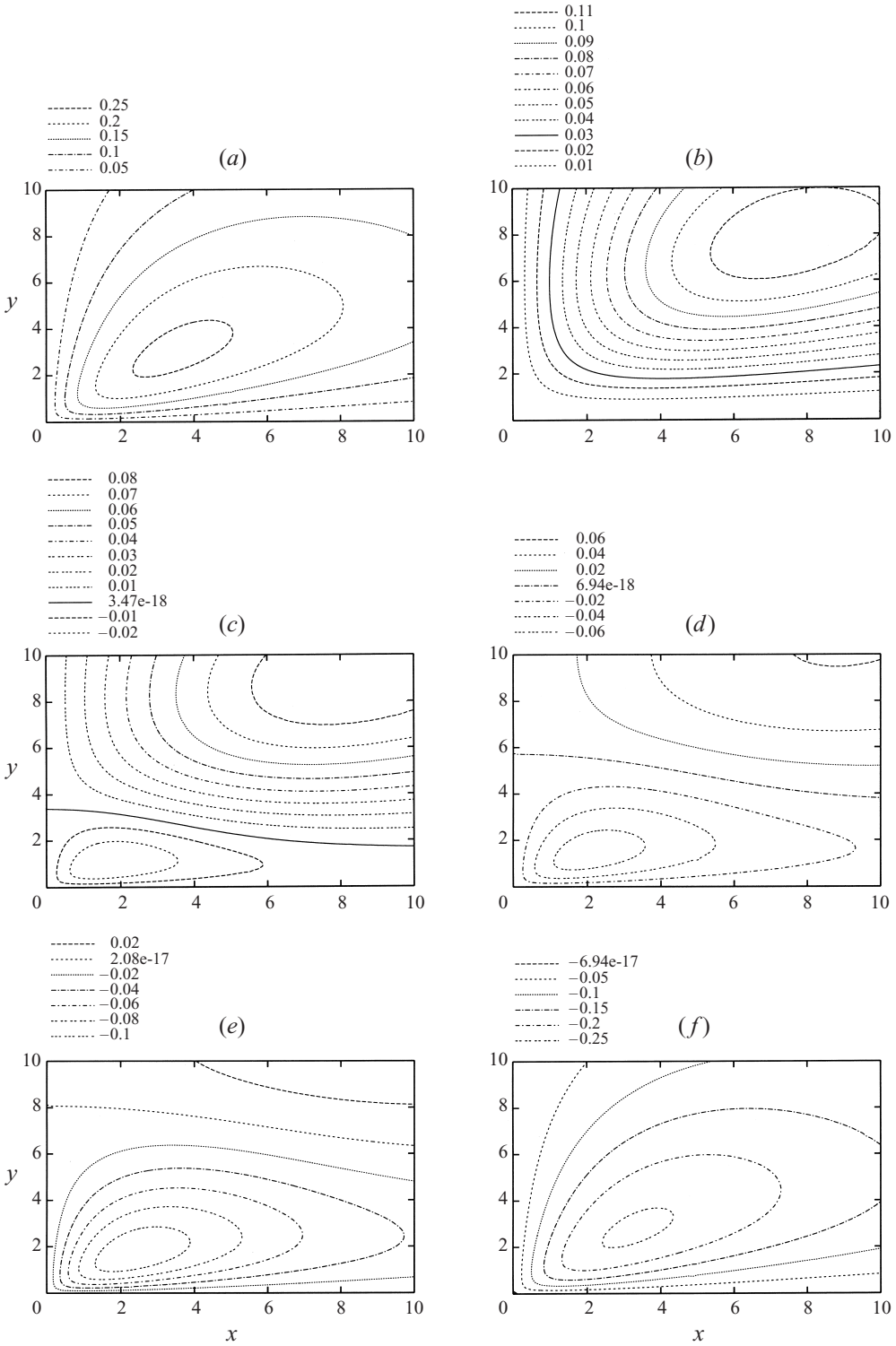


FIGURE 6. Streamlines for the contact-line motion over an oscillating plate with $S = 0.1$ on $0 < x, y < 10$ at times (*a*) $t = \pi/16$, (*b*) $t = \pi/2$, (*c*) $t = 9\pi/16$, (*d*) $t = 5\pi/8$, (*e*) $t = 11\pi/16$, (*f*) $t = \pi$. Notice that from the time the plate reverses direction ($t = \pi/2$), a second vortex begins to develop over the plate, displacing the original flow vertically.

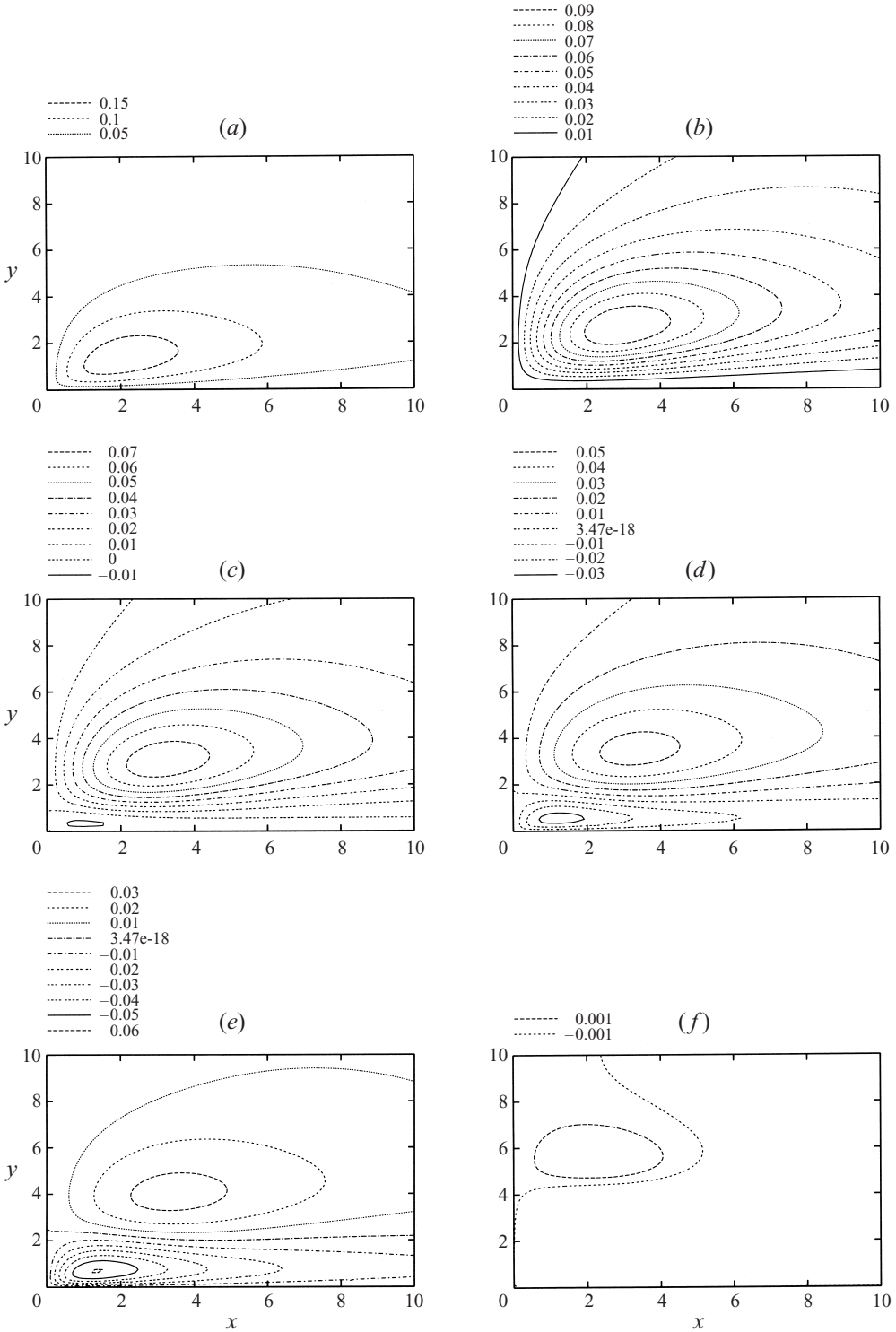


FIGURE 7. Streamlines for the contact-line motion over an oscillating plate with $S = 1$ on $0 < x, y < 10$ at times (*a*) $t = \pi/16$, (*b*) $t = \pi/2$, (*c*) $t = 9\pi/16$, (*d*) $t = 5\pi/8$, (*e*) $t = 11\pi/16$, (*f*) $t = 13\pi/16$. Note that the original flow in (*f*) is completely enclosed in a zero streamline which decays toward the interface as $y \to \infty$.

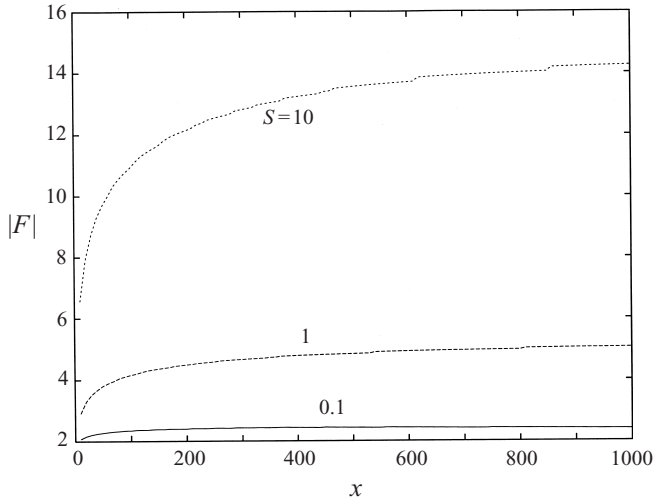


FIGURE 8. Amplitude of the force applied to the plate by the fluid as a function of distance $x$ from the contact line for Strouhal numbers $S = 0.1, 1, 10$.

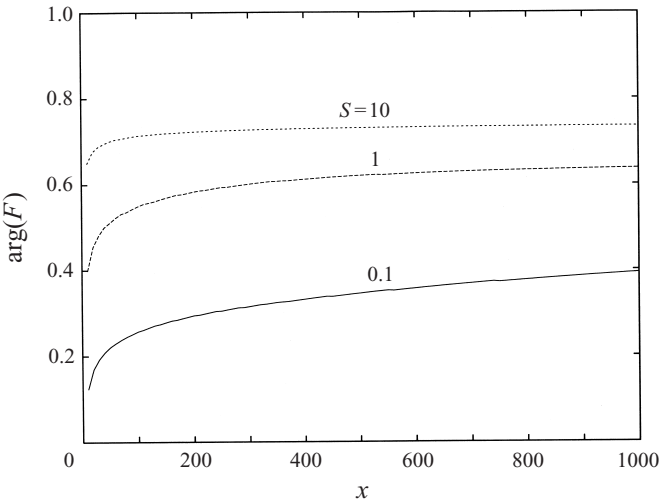


FIGURE 9. Phase difference of the force applied to the plate by the fluid compared to the plate oscillation as a function of distance $x$ from the contact line for Strouhal numbers $S = 0.1, 1, 10$.

and the Laplace transform in $t$, so that

$$\bar{\Theta}_1 = \int_0^\infty \Theta_1(x, y, t) \sin \sigma y \, \mathrm{d}y,$$

$$\hat{\Theta}_1 = \int_0^\infty \bar{\Theta}_1(x, \sigma, t) \mathrm{e}^{-\lambda t} \mathrm{d}t.$$

The solution of the resulting boundary-value problem in $x$ is found to be

$$\bar{\Theta}_1^{(s)}(x, \sigma) = \frac{P}{2\sigma} \int_0^\infty \left\{ \frac{B - \sigma}{B + \sigma} \mathrm{e}^{-(x+\xi)\sigma} - \mathrm{e}^{-|x-\xi|\sigma} \right\} \hat{J}^{(s)}(\xi, \sigma) \, \mathrm{d}\xi \tag{4.2}$$

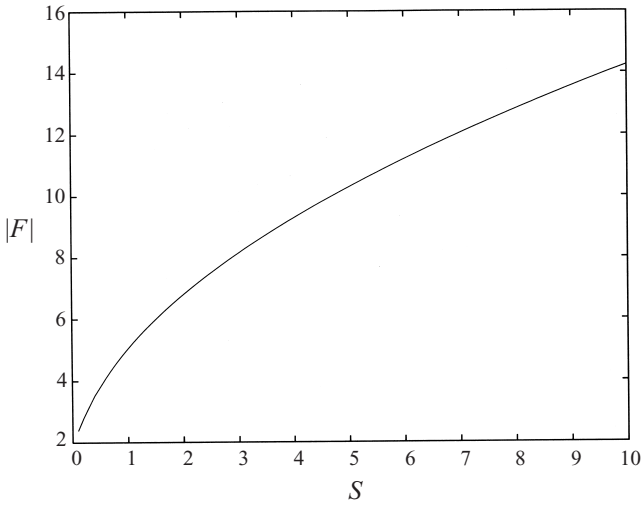


FIGURE 10. Amplitude of the force applied to the plate by the fluid as a function Strouhal number $S$ at a distance $x = 1000$ from the contact line. Note that the square-root behaviour coincides with the dissipation rate $v^{1/2}$ found in other applications.

$$\bar{\Theta}_1^{(u)}(x,\sigma,t) = \mathrm{e}^{\mathrm{i}t}\frac{P}{2\sqrt{\sigma^2+\mathrm{i}SP}}\int_0^\infty \left\{\frac{B-\sqrt{\sigma^2+\mathrm{i}SP}}{B+\sqrt{\sigma^2+\mathrm{i}SP}}\exp(-(x+\xi)\sqrt{\sigma^2+\mathrm{i}SP}) - \exp(-|x-\xi|\sqrt{\sigma^2+\mathrm{i}SP})\right\}\hat{J}^{(u)}(\xi,\sigma)\,\mathrm{d}\xi\,, \quad (4.3)$$

where the superscripts $s$ and $u$ correspond to the steady and unsteady components of the advection term $J(\psi_0,\Theta_0)$. The temperature variations due to Marangoni-induced flow ($\Theta_1^{(s)}$), and the variations due to flow driven by the oscillating plate ($\Theta_1^{(u)}$) can be rewritten in the physical coordinates as convolution integrals over the total wedge

$$\Theta_1^{(s)} = \frac{2P}{\pi}\int_0^\infty\int_0^\infty\int_0^\infty \left\{\frac{B-\sigma}{B+\sigma}\mathrm{e}^{-(x+\xi)\sigma} - \mathrm{e}^{|x-\xi|\sigma}\right\} J(\psi_0^{(s)},\Theta_0)\sin\sigma y\sin\sigma\eta\,\mathrm{d}\sigma\mathrm{d}\eta\mathrm{d}\xi. \quad (4.4)$$

$$\Theta_1^{(u)} = \frac{2Pe^{\mathrm{i}t}}{\pi}\int_0^\infty\int_0^\infty\int_0^\infty \left\{\frac{B-\sqrt{\sigma^2+\mathrm{i}SP}}{B+\sqrt{\sigma^2+\mathrm{i}SP}}\exp(-(x+\xi)\sqrt{\sigma^2+\mathrm{i}SP}) - \exp(|x-\xi|\sqrt{\sigma^2+\mathrm{i}SP})\right\} J(\psi_0^{(u)},\Theta_0)\sin\sigma y\sin\sigma\eta\,\mathrm{d}\sigma\mathrm{d}\eta\mathrm{d}\xi + \text{c.c.} \quad (4.5)$$

Hence, the evaluation of the temperature field requires the triple integration over the domain $(\sigma,\xi,\eta)$. We perform this integration numerically, with the technique described in the Appendix. In the following we present the results for the steady and unsteady $O(Re)$ corrections to the temperature field.

### 4.1. *Steady heat transport*

The steady component of heat transport depends linearly on the Marangoni number and nonlinearly on the Biot number. We examine how the value of $B$ affects heat transport in this subsection.

Figure 11 shows the steady isotherms of the disturbance thermal field for $B = 0.1, 1,$ and 10. In the cases of $B = 1$ and $B = 10$, the magnitude and direction of the induced flow play a role in reducing heat transport from the plate into the bulk. The reverse flow along the plate transports the locally warmer fluid along the plate prior to the advection along the separating streamline. Since the strength of the flow is weak, the thermal conduction time scale is much shorter than that of the advective time scale, leading to poorer heat transport from the plate into the bulk. In the $B = 0.1$ case, the strength of the Marangoni flow is larger, and the advective time scale is shorter, than that of thermal transport, resulting in improved heat transport from the plate into the bulk. In terms of advection increasing heat transport from the plate into the bulk, an insulated interface results in stronger fluid motions induced by Marangoni interfacial stresses. These fluid motions then transport heat effectively from the plate into the bulk. However, we note that these effects are small compared the leading-order temperature field; the degree of heat transport in this case is small compared to the nearly uniform temperature that would result in no heat transport across the interface.

### 4.2. *Unsteady heat transport*

In the unsteady case, heat transport is controlled by the relative size of the inverse of the Biot number and the unsteady thermal diffusive scale $SP$. Again, the solution local to the contact line produces a minimum (or maximum, since we are considering the time-harmonic heat transfer component). The evolution of this minimum depends on the relative sizes of $B^{-1}$ and $SP$. Owing to the large array of possible parameter values, we restricted our study to $B^{-1} = 1$ and $B^{-1} = 10$, which correspond to the values of water and of alcohol, respectively, from Burelbach *et al.* (1988).

When $B^{-1} \ll SP$, heat transport is localized to the contact line and the interface. We show a half-cycle of this solution in figure 12, where $B = P = 1$, $\beta = 0.1$, and $S = 10$. As in the steady heat transport case, the localized sink is found to be near the contact line. As the plate begins to decelerate, this cooled region is carried into the bulk along the interface in a similar path to that of the vortex shown in figure 7, but is not advected due to the large Strouhal number. As the plate decelerates, there is a thermal layer from the interface that is carried into the bulk, nearly uniformly, by the decelerating flow, as is shown in figure 12(*c–e*).

When $B^{-1} \sim SP$, we see that the transport of heat depends on both the interfacial heat transport and advection. Figure 13 shows a half-cycle of the disturbance thermal field, where the localized cooled region propagates into the bulk on roughly a 45° path. The advection of the outer flow acts to cool/heat this region as it propagates, weakening thermal gradients in the bulk.

The case of $B^{-1} \gg SP$ demonstrates how poor thermal conductance by the interface can increase thermal transport into the bulk. As in the $B^{-1} \ll SP$ case, the localized region remains close to the interface during the half-cycle, as is shown in figure 14. However, the region above the plate is heated/cooled at a much higher rate than the localized region moving vertically along the interface. The heat flux through the interface local to the contact line and the heat flux in this region is cooling the fluid above the plate at a much faster rate than in the bulk. In fact, from figure 14, we see that the plate is cooled in the domain in $x$ shown, and that this cooled region is

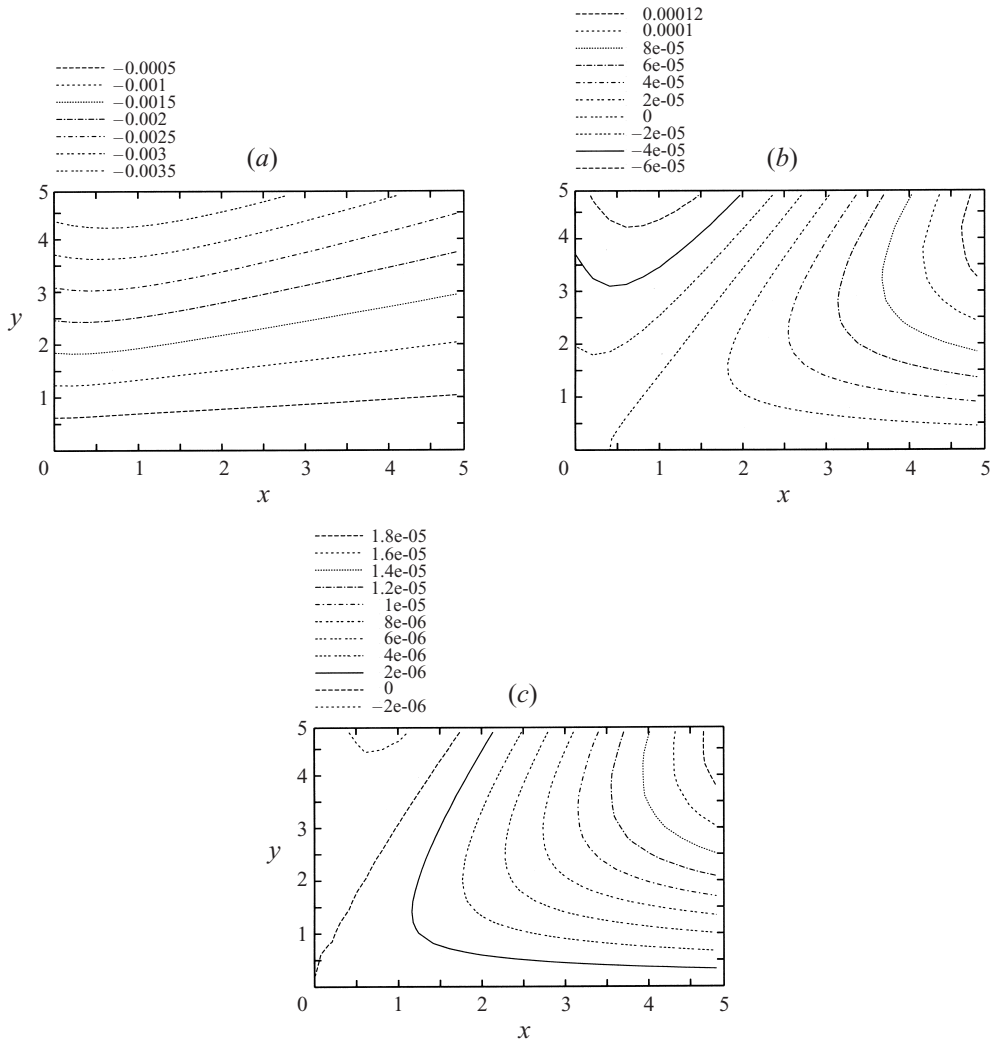


FIGURE 11. Isotherms of the disturbance thermal field induced by the leading-order temperature field and the leading-order flow induced by Marangoni stresses when (*a*) $B = 0.1$, (*b*) $B = 1$, and (*c*) $B = 10$. Note that the best advected heat transport from the plate is for smaller Biot numbers. The reverse flow induced by the Marangoni stresses actually retards heat transport across the plate.

then transported by advection into the bulk as the plate reverses direction. In none of the numerical simulations that were performed, did the ratio of the slip length scale to the thermal boundary-layer scale $\beta$ play a significant role in the qualitative features of the heat transport, or in the quantitative features away from the contact line.

## 5. Conclusions

In this work, we have investigated the fluid flow local to a contact line driven by thermocapillarity and interfacial heat transfer in addition to weak plate oscillations. Since the amplitude of both forced flows is small, inertial effects are much smaller

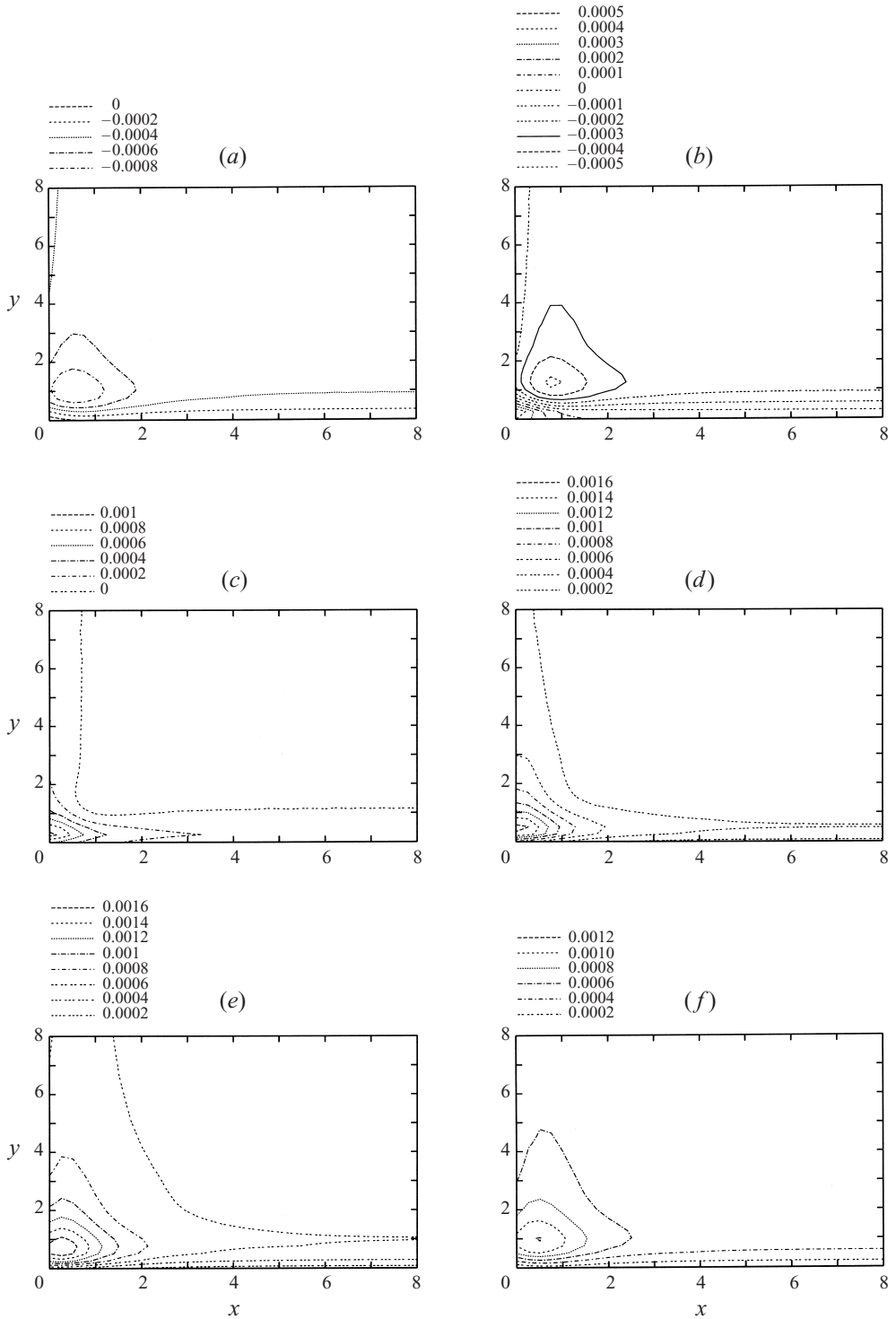


FIGURE 12. Half-cycle of the time-harmonic portion of the temperature field with $B = P = 1, S = 10$ with (*a*) $t = 0$, (*b*) $t = \pi/8$, (*c*) $t = \pi/4$, (*d*) $t = 7\pi/32$, (*e*) $t = 3\pi/4$, and (*f*) $t = 15\pi/16$. Heat transport is advected from the interface into the bulk as the plate reverses direction.

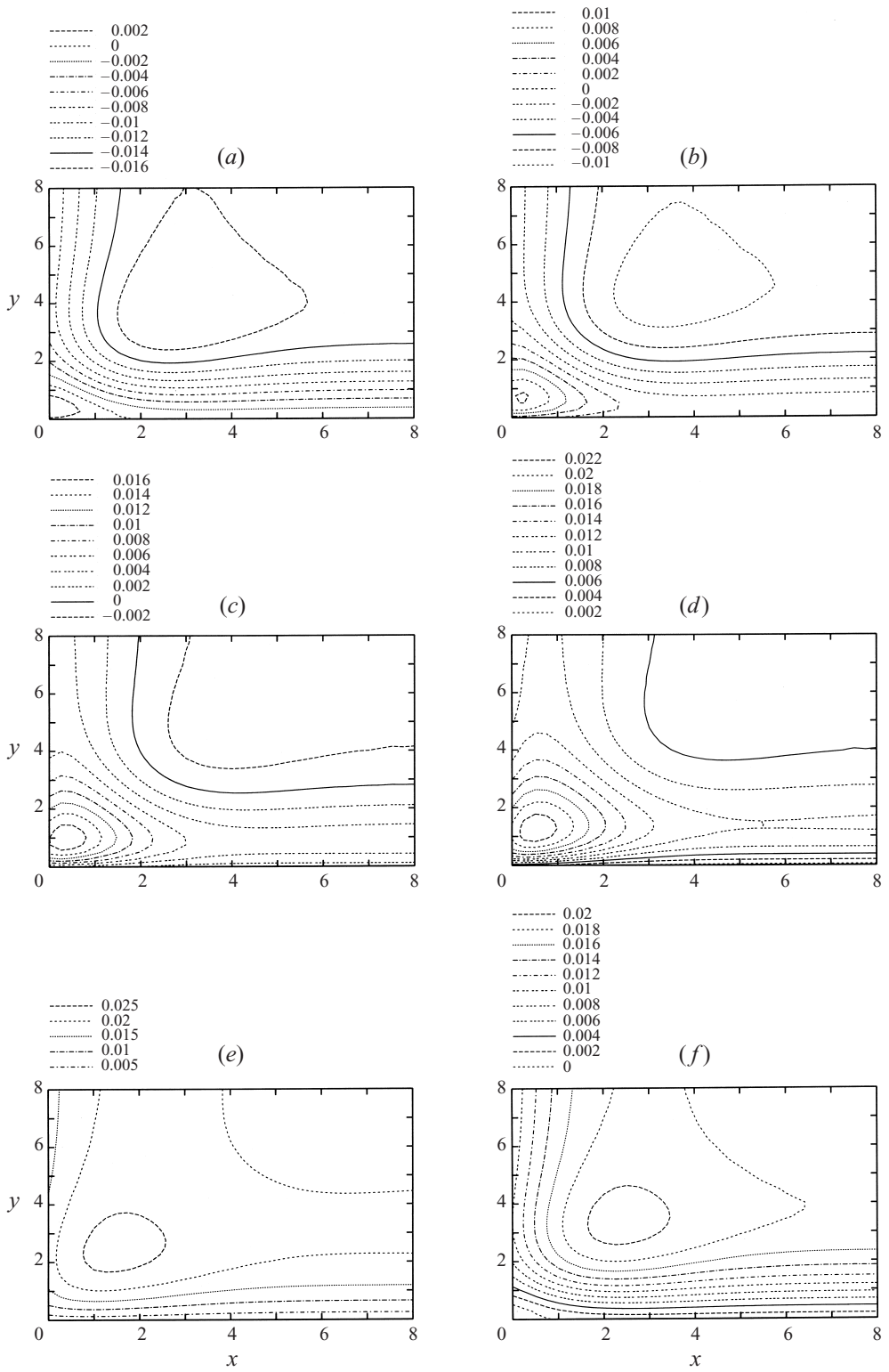


FIGURE 13. For caption see facing page.

than viscous and unsteady effects, and the heat and momentum equations decouple. This allows the solution of each flow separately, and the superposition of the two flows gives the total leading-order flow.

In the thermally driven problem, deviation from equilibrium leads to non-zero temperature gradients along the interface. Since surface tension depends on temperature, these deviations result in a non-zero tangential stress at the interface, inducing a flow within the bulk. The temperature profile is found to have a localized heated region near the contact line which scales on the thermal boundary layer. Outside this region the fluid remains above the ambient temperature, but approaches the ambient temperature along the interface far from the contact line. This interfacial temperature profile thus induces two regions of flow: a stagnation-type flow along the interface into the contact-line region, which separates from the plate, the separation point scaling inversely with Biot number; and a flow reversal region that brings liquid along the plate to the separation point and up along the separating streamline. The force that the fluid applies to the plate is governed primarily by the second region. The reverse flow acts to increase the negative force along the plate. In the thermally insulated interface case, there is no reverse flow and the force on the plate remains bounded. Further, we find that the liquid velocity along the interface near the contact line, to leading order in distance from the contact line, is non-uniform and that this term does not depend on the Biot number.

When an isothermal fluid on an oscillating plate moves locally to a contact line, no systematic method of finding an appropriate slip law is possible, and we have used a simple separable slip law to describe the flow local to an oscillatory contact line. We find that the long-time solution of the flow results in the formation of vortices during the plate reversal; these vortices propagate and dissipate into the bulk as the plate accelerates. The vertical dissipation length scale of the vortex scales as $S^{-1/2}$, i.e. within the Stokes boundary layer. Interfacial velocity local to the contact line resembles the prescribed slip law along the plate with a phase shift that is Strouhal-number dependent.

This flow is then used to determine the modification of heat transfer by considering the correction to the thermal field (assuming that the interface remains flat at $O(Re)$ as well). From the time-harmonic component of the solution, interfacial heat transfer acts to transport heat from the plate. As the plate reverses direction, this cooled region is then carried into the bulk. Note that the inverse of the Biot number corresponds to the degree of disequilibrium of the liquid, suggesting that liquids with large values of $B^{-1} = K$ may enhance heat transport from the plate into the bulk.

This work was sponsored by a grant from the Office of Basic Energy Sciences, US Department of Energy, and from grant from the National Science Foundation (DMS-9971383). B.S.T. would also like to thank Professor Michael J. Miksis for some interesting discussions. We would also like to thank one of the referees who recognized a flaw in the original version of this manuscript.

FIGURE 13. Half-cycle of the time-harmonic portion of the temperature field with $B = S = P = 1$ with (*a*) $t = 0$, (*b*) $t = \pi/8$, (*c*) $t = \pi/4$, (*d*) $t = 3\pi/8$, (*e*) $t = 3\pi/4$, and (*f*) $t = 15\pi/16$. Notice that the cooled region local to the contact line propagates into the bulk at approximately an angle of $\pi/4$, suggestive of the balance of heat transfer and advection.

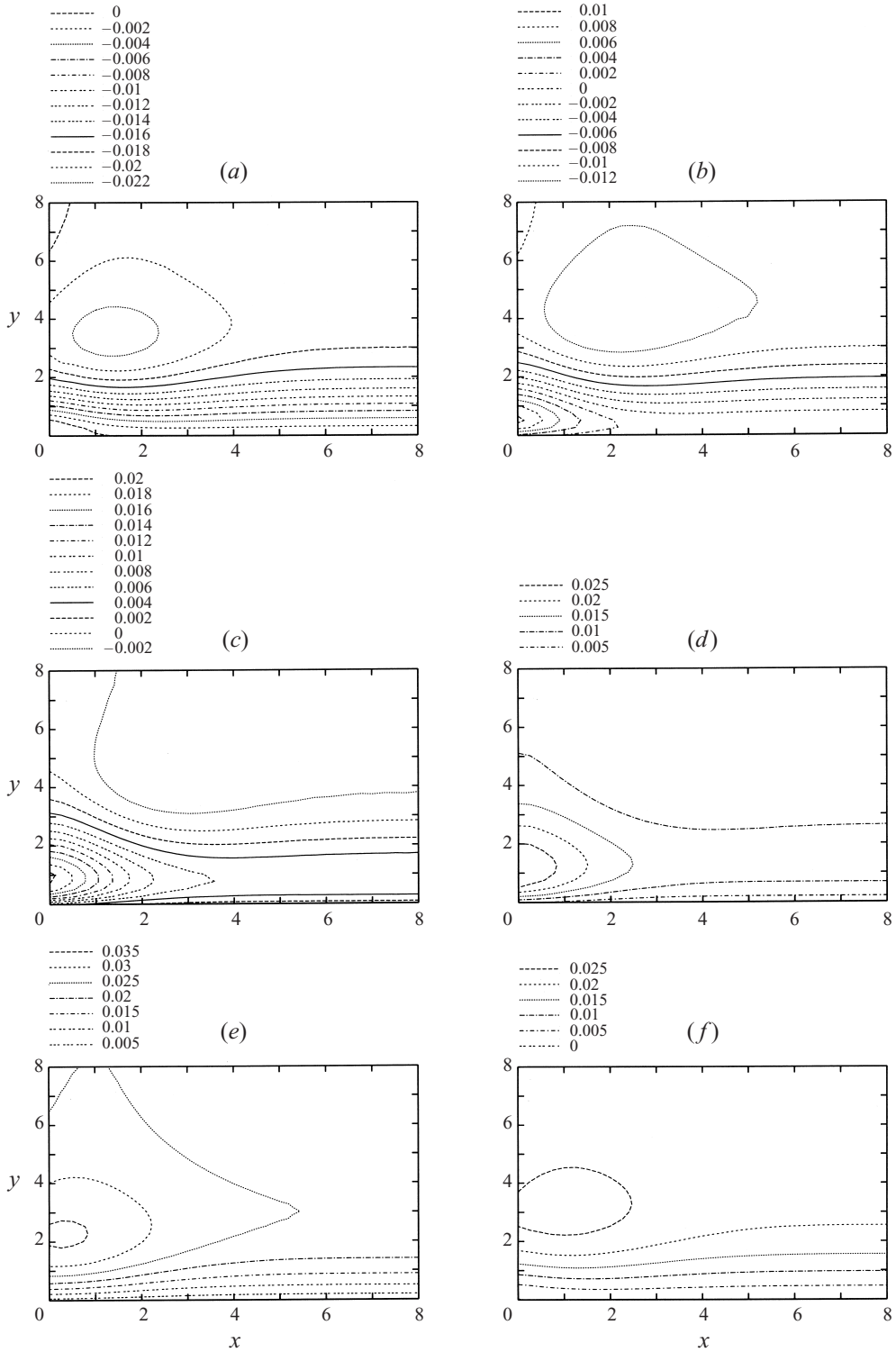


FIGURE 14. For caption see facing page.

## Appendix. Description of the numerical method to determine $\Theta_1$

In order to find the $O(Re)$ correction to the thermal field, we needed to efficiently find solutions to integrals of the form

$$I(x, y) = \int_0^\infty \int_0^\infty \int_0^\infty K(x, y, \xi, \eta, \sigma)\, \mathrm{d}\sigma \mathrm{d}\eta \mathrm{d}\xi. \tag{A 1}$$

The motivation for performing numerical solutions of such integrals rather than a direct numerical simulation is that the boundary conditions far from the contact line are not known. In fact, they can only be determined from a matched asymptotic analysis of some specific outer flow, but it can be shown that these integrals do converge for finite $(x, y)$. Inappropriate boundary conditions, especially in the time-harmonic case, can lead to spurious results. So although the numerical technique described below is less efficient than some direct numerical techniques, errors induced by boundary conditions have been completely eliminated.

Further, the kernel $K(x, y, \xi, \eta, \sigma)$ decays either exponentially or algebraically in $\sigma$ in an oscillatory fashion. To find the integral in $\sigma$ to high accuracy, typically to within $10^{-11}$, the domain of integration is partitioned into half-periods of the fastest oscillation, and the integral is calculated in this period with Gaussian quadrature (typically 20 points are used on a domain of length $\pi$). In the steady case, adaptive quadrature was used to resolve the flow-field convolution of the interfacial temperature in each of these domains. Each partial sum of this integral provides a sequence of the full integral, and this sequence is accelerated using Padé approximants in a continued-fraction formulation (see Chisholm, Genz & Rowlands 1972 and Blakemore, Evans & Hyslop 1976). Convergence within tolerance was found, typically, in about six iterates (or integrating to about $12\pi$ in the domain), even for the algebraically decaying case. The region near $\xi = x, \eta = y$, at which $K(x, y, \xi, \eta, \sigma)$ has a logarithmic singularity, was excluded. The error in the final integral can be shown to scale on the area of the excluded region, and hence we choose the scale of this region so that this contribution to the error is within the tolerance for $I$. The remaining integration in $\xi, \eta$ is done using polar coordinates $r, \phi$ for which Gaussian quadrature is used in $\phi$, with four Gaussian points added the azimuthal grid for each unit $r$, and Padé approximants used in $r$ to accelerate the convergence *after* the region near $(x, y)$ had been integrated. Twenty Gaussian points per unit $r$ were used in each of the partial sum calculations. Typical runs for the generation of $\hat{\Theta}_1$ on a $32 \times 32$ grid to within $10^{-6}$ accuracy took on the order of a single CPU day on a R12000 Silicon Graphics processor. The degree of accuracy at each point allows us to use a coarse grid on $(x, y)$ and standard interpolation packages for the determination of the thermal field correction.

## REFERENCES

Anderson, D. M. & Davis, S. H. 1993 Two-fluid viscous flow in a corner. *J. Fluid Mech.* **257**, 1.

Anderson, D. M. & Davis, S. H. 1994 Local fluid and heat flow near contact lines. *J. Fluid Mech.* **268**, 231.

Figure 14. Half-cycle of the time-harmonic portion of the temperature field with $B = 0.1, S = P = 1$ with (*a*) $t = 0$, (*b*) $t = \pi/8$, (*c*) $t = \pi/4$, (*d*) $t = 3\pi/8$, (*e*) $t = 3\pi/4$, and (*f*) $t = 15\pi/16$. Notice that the localized cooled region propagates along the plate into the bulk prior to be advected. This is suggestive of how a thermally 'insulated' interface can enhance heat transport away from the plate and into the bulk.

Benjamin, T. B. & Scott, J. C. 1979 Gravity-capillary waves with edge constraints. *J. Fluid Mech.* **92**, 241.

Blakemore, M., Evans, G. A. & Hyslop, J. 1976 Comparison of some methods for evaluating infinite range oscillatory integrals. *J. Comput. Phys.* **22**, 352.

Burelbach, J. P., Bankoff, S. G. & Davis, S. H. 1988 Nonlinear stability of evaporating/condensing liquid films. *J. Fluid Mech.* **195**, 463.

Chisholm, J. S. R., Genz, A. & Rowlands, G. E. 1972 Accelerated convergence of sequences of quadrature approximations. *J. Comput. Phys.* **10**, 284.

Cox, R. G. 1986 The dynamics of the spreading of liquids on a solid surface. Part I. Viscous flow. *J. Fluid Mech.* **168**, 169.

Davis, S. H. 1983 Contact-line problems in fluid mechanics. *Trans. ASME: J. Appl. Mech.* **50**, 997.

Dussan V., E. B. 1976 Contact-line motion of a steadily moving plate. *J. Fluid Mech.* **77**, 665.

Dussan V., E. B. & Davis, S. H. 1974 On the motion of a fluid-fluid interface along a solid surface. *J. Fluid Mech.* **65**, 71.

Goodwin, R. & Homsy, G. M. 1991 Viscous flow down a slope in the vicinity of a contact line. *Phys. Fluids* A **3**, 51.

Henderson, D. M. & Miles, J. W. 1994 Surface-wave damping in a circular cylinder. *J. Fluid Mech.* **275**, 285.

Hocking, L. M. 1987*a* The damping of capillary-gravity waves at a rigid boundary. *J. Fluid Mech.* **179**, 253.

Hocking, L. M. 1987*b* Waves produced by a vertically oscillating plate. *J. Fluid Mech.* **179**, 267.

Martel, C., Nicolás, J. A. & Vega, J. M. 1998 Surface-wave damping in a brimful circular cylinder. *J. Fluid Mech.* **360**, 213.

Mei, C. C. & Liu, L. F. 1973 The damping of surface gravity waves in a bounded liquid. *J. Fluid Mech.* **59**, 239.

Miksis, M. J. & Davis, S. H. 1994 Slip over rough and coated surfaces. *J. Fluid Mech.* **273**, 125.

Miles, J. 1990*a* Parametrically excited standing edge waves. *J. Fluid Mech.* **214**, 43.

Miles, J. 1990*b* Wave reflection from a gently sloping beach. *J. Fluid Mech.* **214**, 59.

Miles, J. 1991 Wave motion in a viscous fluid of variable depth. Part 2. Moving contact line. *J. Fluid Mech.* **223**, 47.

Miles, J. W., & Henderson, D. M. 1998 A note on interior vs. boundary-layer damping of surface waves in a circular cylinder. *J. Fluid Mech.* **364**, 319.

Perlin, M. & Schultz, W. W. 2000 Capillary effects on surface waves. *Ann. Rev. Fluid Mech.* **32**, 241.

Press, W. H., Teukolsky, S. A., Vetterling, W. T. & Flannery, B. P. 1992 *Numerical Recipes, The Art of Scientific Computing*. Cambridge University Press.

Sheng, P. & Zhou, M. 1992 Immiscible-fluid displacement: Contact-line dynamics and the velocity-dependent capillary pressure. *Phys. Rev.* A **45**, 5694.